

# Theoretical Treatments of the Bound-Free Contribution and Experimental Best Practice in X-ray Thomson Scattering from Warm Dense Matter

Brian A. Mattern<sup>1</sup> and Gerald T. Seidler<sup>1, a)</sup>

*Department of Physics, University of Washington, Seattle, WA 98195-1560*

(Dated: 15 October 2018)

By comparison with high-resolution synchrotron x-ray experimental results, we assess several theoretical treatments for the bound-free (core-electron) contribution to x-ray Thomson scattering (i.e., also known as nonresonant inelastic x-ray scattering). We identify an often overlooked source of systematic error in the plane-wave form factor approximation (PWFFA) used in the inference of temperature, ionization state, and free electron density in some laser-driven compression studies of warm dense matter. This error is due to a direct violation of energy conservation in the PWFFA. We propose an improved practice for the bound-free term that will be particularly relevant for XRTS experiments performed with somewhat improved energy resolution at the National Ignition Facility or the Linac Coherent Light Source. Our results raise important questions about the accuracy of state variable determination in XRTS studies, given that the limited information content in low-resolution XRTS spectra does not strongly constrain the models of electronic structure being used to fit the spectra.

## I. INTRODUCTION

The field of *warm dense matter* (WDM) rests in the transitional regime between traditional condensed phase systems and strongly-correlated, fully-ionized plasmas. As such, it draws from the complexity of both fields while showing its own special fundamental and, as we show here, pragmatic challenges. A significant and growing literature exists on the electronic structure,<sup>1–5</sup> thermodynamics<sup>6</sup> and hydrodynamics<sup>7</sup> of WDM, in addition to a range of applications in fusion energy science<sup>8</sup> and laboratory astrophysics.<sup>9,10</sup> Here, however, we investigate a particular difficulty of the WDM regime: assessing the accuracy of the experimental determination of the basic state variables of the system, such as temperature, density and ionization state. Reliable inference of these quantities is central to the clearly-needed improvements in the equation of state of materials under, for example, the entire range of conditions leading from ambient matter to inertial confinement fusion.<sup>11</sup>

The high optical opacity of WDM requires the use of penetrating probe radiation, i.e., x-ray photons with energies of a few to a few tens of keV. Unfortunately, with only few counterexamples<sup>12</sup> the inference of state-variables using these methods is limited by the degree of understanding of the electronic structure of WDM and its relationship to the state variables themselves. Faintly circular co-dependencies of this type are not uncommon in emergent fields of experimental science (e.g., consider the many years of effort needed to establish accurate and precise pressure sensing in the Mbar range in opposed-anvil pressure cells<sup>13–16</sup>), and a firm foundation for such methodologies can follow from any of several developments. Foremost among such developments are: experimental data of sufficient information content to it-

self strongly constrain the constituent theories for electronic structure; broad programs to assess accuracy by cross-comparison of different metrologies; and, finally, an eventual comparison to international standards. The experimental determination of state variables in the WDM regime is seeing only the earliest such examples, including notably the rare experiments using detailed balance in x-ray Thomson scattering<sup>12</sup> or the recent checks in consistency between conclusions drawn from the elastic and inelastic components of x-ray scattering.<sup>17</sup>

The present paper reports a first step in evaluating the accuracy, rather than precision, of the methods used for state variable determination in the WDM regime. To this end, we investigate the various available treatments for the core-electron, or bound-free, contribution to x-ray Thomson scattering (XRTS, also called nonresonant inelastic x-ray scattering, NIXS<sup>18</sup>) with a special emphasis on the plane-wave form-factor approximation (PWFFA) of Schumacher, et al.<sup>19</sup>. We will show that this approximation, which has seen extensive use in XRTS studies of shock-compressed matter,<sup>17,20–25</sup> is fundamentally flawed and presents a source of systematic uncertainty in inferred quantities.

Based on these observations we come to three main conclusions. First, looking to the near future, when XRTS studies of WDM with improved energy resolution will be performed at the Linac Coherent Light Source<sup>26</sup> and the National Ignition Facility<sup>11</sup>, the errors implicit in the use of the PWFFA must be avoided if physically meaningful information on the equation of state in the WDM regime is to be determined. Second, while it is important to note that a faulty theoretical treatment has been used, and that some reevaluation of experimental results may be called for, the more lasting conclusion is that the information content in the measured XRTS spectra for WDM has been insufficient to alert the experimenters to the presence of an unphysical model for the electronic structure. This strongly suggests the need for cross-comparison with alternative methods of

<sup>a)</sup>Electronic mail: seidler@uw.edu

WDM state variable determination, e.g., x-ray fluorescence thermometry<sup>27–32</sup>. Third, we find that stronger connections between the synchrotron x-ray and WDM-XRTS communities provide important experimental and theoretical synergies. The wealth of very high-resolution studies at synchrotron light sources of both the free-free (valence)<sup>33–40</sup> and bound-free (core)<sup>18,41–53</sup> contributions to XRTS provide important benchmarks both for comparison to WDM-specific theory and also for validation of experimental protocol including, e.g., instrument-specific backgrounds. Further, as we have illustrated here, there will be cases where theoretical methods already in use for synchrotron studies may be beneficially transported to WDM-XRTS studies.

In Sect. II we discuss four theoretical treatments of bound-free XRTS: the impulse approximation (IA), which is valid at large energy transfer; a hydrogenic model (HM); an extension of the IA to incorporate binding energies (PWFFA); and a real-space Green's function method (RSGF). The first three are essentially atomic (with varying degrees of approximation), while the latter treats the condensed solid, and is based on methods broadly used for many years in the interpretation of several x-ray spectroscopic techniques.<sup>54,55</sup>

Since high-resolution XRTS data from WDM at known thermodynamic conditions is currently unavailable, we instead compare each of the above theories with very high-quality XRTS spectra collected under ambient conditions at a synchrotron x-ray source. This provides a baseline validation for the core contribution: a theoretical treatment which fails under these conditions is certain to form a weak foundation when including the further complexities of continuum lowering and partial ionization present in WDM.

Experimental details are described in Sect. III and the comparison of theory and experiment is made in Sect. IV A. The relative success of even atomic treatments at describing the condensed solid suggests that these methods should be extensible to the WDM regime with only minor modifications. However, we find that the PWFFA, which has been used for a few years in the interpretation of WDM measurements,<sup>17,20–25</sup> is in stark disagreement with the ambient experimental data. In Sect. IV B, we show that this disagreement is due to internal inconsistency in the PWFFA that leads to unphysical results. Next, in Sect. IV C, we consider the implications of using the PWFFA to model the bound-free contribution to WDM XRTS data; namely, the likelihood of previously-undiagnosed systematic errors in extracted thermodynamic quantities. These observations then motivate a discussion of best future practice in Sect. IV D, after which we conclude in Sect. V.

## II. THEORY

The fundamental observable in XRTS/NIXS is the *dynamic structure factor*  $S(\vec{q}, \omega)$ , which separates into inde-

pendent contributions from electrons in different shells. We will focus on the contribution from tightly bound core electrons, i.e., the *bound-free* contribution. The theoretical description of bound-free XRTS begins with the Kramers-Heisenberg formula for the first-Born approximation to the double-differential scattering cross-section (DDSCS):<sup>18</sup>

$$\frac{d^2\sigma}{d\omega d\Omega} = \frac{\omega_2}{\omega_1} r_o^2 |\hat{\epsilon}_1 \cdot \hat{\epsilon}_2^*|^2 S(\vec{q}, \omega) \quad (1)$$

$$S(\vec{q}, \omega) = \sum_I P_I(T) \sum_F \left| \langle F | \sum_j e^{i\vec{q} \cdot \vec{r}_j} | I \rangle \right|^2 \times \delta(E_F - E_I - \omega) \quad (2)$$

Here,  $\omega_{1,2}$  and  $\hat{\epsilon}_{1,2}$  are initial and final photon energies and polarizations;  $r_o$  is the Thomson scattering length;  $|I\rangle, |F\rangle$  are initial and final many-body states with energies  $E_I, E_F$ ;  $P_I(T)$  is the temperature-dependent Boltzmann factor;  $\vec{q}$  is the momentum transfer;  $\omega = \omega_1 - \omega_2$  is the energy transfer and  $j$  indexes individual electrons. In this and subsequent formulae, we use Hartree atomic units ( $\hbar = m_e = 1$ ).

In the independent particle approximation, Eq. (2) can be written as

$$S(\vec{q}, \omega) = \sum_i n_i S_i(\vec{q}, \omega) \\ S_i(\vec{q}, \omega) = \sum_f (1 - n_f) \left| \langle f | e^{i\vec{q} \cdot \vec{r}} | i \rangle \right|^2 \delta(E_f - E_i - \omega) \quad (3)$$

where  $|i\rangle, |f\rangle$  are initial and final state *single particle* states with energies  $E_i, E_f$  and thermally-averaged occupation numbers  $n_i, n_f$ .

### A. The impulse approximation

In the limit of large energy-transfer  $\omega$  relative to the initial state binding energy  $E_B$ , known as the impulse approximation (IA), the XRTS spectrum is completely determined by the initial-state electronic momentum distribution; the binding energy of the scattering electron plays no role.<sup>56</sup>

For  $\omega \gg E_B$ , only unoccupied final states contribution to Eq. (3), so we set  $n_f = 0$ . Next, following Eisenberger and Platzman,<sup>56</sup> we expand the  $\delta$ -function using the standard Fourier representation

$$\delta(\omega) = \int \frac{dt}{2\pi} e^{i\omega t}. \quad (4)$$

After rearranging slightly and using the fact that  $|i\rangle$  and  $|f\rangle$  are eigenstates of the single-particle Hamiltonian  $H$ , we find

$$S_i(\vec{q}, \omega) = \int \frac{dt}{2\pi} \sum_f e^{i\omega t} \langle i | e^{iHt} e^{-i\vec{q} \cdot \vec{r}} e^{-iHt} | f \rangle \langle f | e^{i\vec{q} \cdot \vec{r}} | i \rangle \\ = \int \frac{dt}{2\pi} e^{i\omega t} \langle i | e^{iHt} e^{-i\vec{q} \cdot \vec{r}} e^{-iHt} e^{i\vec{q} \cdot \vec{r}} | i \rangle. \quad (5)$$

In the second line, we have used completeness to remove the sum over final states. The IA corresponds to replacing  $H$  by the free-particle Hamiltonian  $H_0$ , which can be justified in the limit of  $(\omega/E_B)^2 \gg 1$  (see Section III of Ref. 56). After inserting a complete set of momentum eigenstates and integrating over the direction of momentum, we obtain

$$S_i(\vec{q}, \omega) = (2\pi/q) \int_{|w/q-q/2|}^{\infty} p dp \rho_i(p), \quad (6)$$

where  $\rho_i(p) = (2\pi)^{-3} |\langle i|p\rangle|^2$  is the initial-state momentum density, which is here assumed to be isotropic (e.g.  $s$ -shell, or sum over a filled subshell).

This formula can be interpreted as describing XRTS from a gas of free electrons with the same initial-state momentum distribution. The scattering spectrum consists of a line centered at the free-particle Compton shift  $\omega_c = q^2/2$  that is Doppler broadened by the projection of the momentum distribution along the direction of  $\vec{q}$ . The integral over the momentum distribution in Eq. (6) simply counts electrons with a given momentum-projection  $p_q$  determined by the energy transfer.

We now turn to methods that take the binding energy into account.

## B. Hydrogenic Model

It is possible to analytically evaluate Eq. (3) using hydrogenic initial and final states. For a  $1s$  initial state, the result is<sup>56</sup>

$$S_i(q, \omega) = \int \frac{d^3p}{(2\pi)^3} |\langle f|e^{i\vec{q}\cdot\vec{r}}|i\rangle|^2 \delta(\omega - E_B - p^2/2), \quad (7)$$

with

$$\begin{aligned} |\langle f|e^{i\vec{q}\cdot\vec{r}}|i\rangle|^2 &= \frac{\pi^2 8^3 a^2}{p} (1 - e^{-2\pi/pa})^{-1} \\ &\times \exp\left[\frac{-2}{pa} \tan^{-1}\left(\frac{2pa}{1 + (q^2 a^2) - p^2 a^2}\right)\right] \\ &\times [k^4 a^4 + (1/3)k^2 a^2 (1 + p^2 a^2)] \\ &\times [(k^2 a^2 + 1 - p^2 a^2)^2 + 4p^2 a^2]^{-3}. \end{aligned} \quad (8)$$

Here,  $p$  is the final-state momentum,  $a = 1/Z$  where  $Z$  is the effective nuclear charge<sup>57</sup>, and  $E_B = 1/2Z^2$  is the binding energy. In this expression, contributions from bound final states have been neglected. Expressions for shells other than the  $1s$  are included in Schumacher, et al.<sup>19</sup>, where this method is referred to as the *hydrogenic form-factor approximation*. We will, however, refer to this simply as the hydrogenic model (HM).

## C. Plane-wave form-factor approximation

The *plane-wave form-factor approximation* (PWFFA) is an attempt to improve the IA by including the bind-

ing energy in the kinematics. The final states are assumed to be momentum eigenstates, which is conceptually appealing in the context of dense plasmas where the jellium model has found wide application. However, as we demonstrate in Sect. IV B, a fundamental difficulty arises: this approximation effectively evaluates the initial-state energy using the atomic Hamiltonian, while evaluating the final-state energy using the free-particle Hamiltonian. This inconsistent treatment violates energy conservation, resulting in violations of the Bethe  $f$ -sum rule and deviations from experimental results that, although small in the original context of gamma-ray scattering, are quite large under the kinematic conditions typical of XRTS measurements. It is the use of the PWFFA in the interpretation of recent XRTS experiments on WDM<sup>17,20-25</sup> that motivates the present paper.

Schumacher's derivation of the PWFFA<sup>19</sup> makes the following assumptions:

$$\begin{aligned} |f\rangle &= |\vec{p} + \vec{q}\rangle \\ \sum_f &\rightarrow \int \frac{d^3p}{(2\pi)^3} \\ E_f &= E_{\vec{p}+\vec{q}} = \frac{(\vec{p} + \vec{q})^2}{2} \\ E_i &= -E_B \end{aligned} \quad (9)$$

where  $E_B$  is the initial-state binding energy,  $\vec{p}$  is the initial-state momentum and  $\vec{p} + \vec{q}$  is the final-state momentum. Assuming that  $T = 0$  and applying (9) to (3), we find

$$\begin{aligned} S_i(\vec{q}, \omega) &= \int \frac{d^3p}{(2\pi)^3} |\langle \vec{p} + \vec{q} | e^{i\vec{q}\cdot\vec{r}} | i \rangle|^2 \delta(E_{\vec{p}+\vec{q}} + E_B - \omega) \\ &= \int \frac{d^3p}{(2\pi)^3} |\langle \vec{p} | i \rangle|^2 \delta(E_{\vec{p}+\vec{q}} + E_B - \omega) \\ &= \int d^3p \rho_i(\vec{p}) \delta(E_{\vec{p}+\vec{q}} + E_B - \omega) \end{aligned} \quad (10)$$

In the second line we use the fact that  $e^{i\vec{q}\cdot\vec{r}}$  is a momentum translation operator. The last line uses the definition of the momentum density  $\rho_i(\vec{p}) = (2\pi)^{-3} |\langle \vec{p} | i \rangle|^2$ . Furthermore, if we again restrict ourselves to an isotropic momentum density (e.g.,  $s$ -shell, or sum over a filled subshell), we can perform the angular integrals to obtain

$$S_i(\vec{q}, \omega) = (2\pi/q) \int_{|\sqrt{2(\omega-B)}-q|}^{\sqrt{2(\omega-B)}+q} p dp \rho_i(p) \quad (11)$$

This expression, along with (1) differs from Schumacher's<sup>19</sup> Eqs. (5) and (21) only in that it does not contain the relativistic prefactor  $\sqrt{1 + (p/mc)^2}$ , which for the experimental conditions under consideration differs negligibly from unity.

Eq. (11) has the same form as the IA expression Eq. (6), differing only by the bounds on the integration over the momentum density. Given this similarity and the well-tested validity of the IA in its regime of applicability, one would expect that for  $\omega \gg E_B$  the PWFFA

would reproduce the IA. This is, however, not the case — despite claims in the literature to the contrary.<sup>19,23</sup> We will return to this point in Sect. IV, after comparison with experiment.

#### D. The real-space Green's function method

The prior methods have all treated XRTS for an isolated atom to various degrees of approximation. The next method we describe treats an arbitrary cluster of atoms using a real-space Green's function (RSGF) formalism implemented in recent versions of the x-ray spectroscopy code FEFF.<sup>58</sup> This formalism, which can treat complex, aperiodic systems, has been extensively applied to condensed-matter systems, where XRTS/NIXS provides a bulk-sensitive alternative to, and extension of, soft x-ray absorption spectroscopy,<sup>49,58–63</sup> The RSGF approach has recently been extended to treat the valence contribution.<sup>64</sup>

Starting with a description of atomic species and locations, an effective one-particle Green's function for the valence electrons in the cluster of atoms is calculated in the muffin-tin approximation, including the effects of full multiple scattering<sup>55</sup>. This Green's function implicitly contains the excited electronic states that are the final states in the scattering experiment. In terms of a spectral density matrix defined by  $\rho(E) = \sum_f |f\rangle \langle f| \delta(E - E_f)$ , which is related to the Green's function by  $\langle \vec{r} | \rho(E) | \vec{r}' \rangle = -(1/\pi) \text{Im} G(\vec{r}', \vec{r}, E)$ , Eq. (3) can be recast as

$$S_i(\vec{q}, \omega) = \langle i | e^{-i\vec{q}\cdot\vec{r}'} P \rho(E) P e^{i\vec{q}\cdot\vec{r}} | i \rangle. \quad (12)$$

Here  $E = \omega + E_i$  is the photoelectron energy and  $P$  projects the final states (which are calculated in the presence of a core hole) onto the unoccupied states of the initial-state Hamiltonian (which has no core hole).<sup>58</sup> The Green's function can be separated into contributions from the central atom and from scattering off other atoms in the cluster. Likewise, the dynamic structure factor can be factored as

$$S_i(\vec{q}, \omega) = S_0(q, \omega)[1 + \chi_{\vec{q}}(\omega)], \quad (13)$$

where  $S_0(q, \omega)$  is a smoothly varying, isotropic atomic background and  $\chi_{\vec{q}}$  is the fine structure due to all orders of photoelectron scattering from the environment.<sup>50,58</sup> Implicit in the fine structure is information about nearest-neighbor distances and thus also density<sup>58</sup>. However, at the poor experimental resolution typical of WDM measurements<sup>23</sup>, this structure will be washed out. Thus, for our purposes, we will include only the atomic background contribution,  $S_0(q, \omega)$ .

### III. EXPERIMENT

Although we are ultimately interested in the elevated temperatures and densities of WDM, it is important

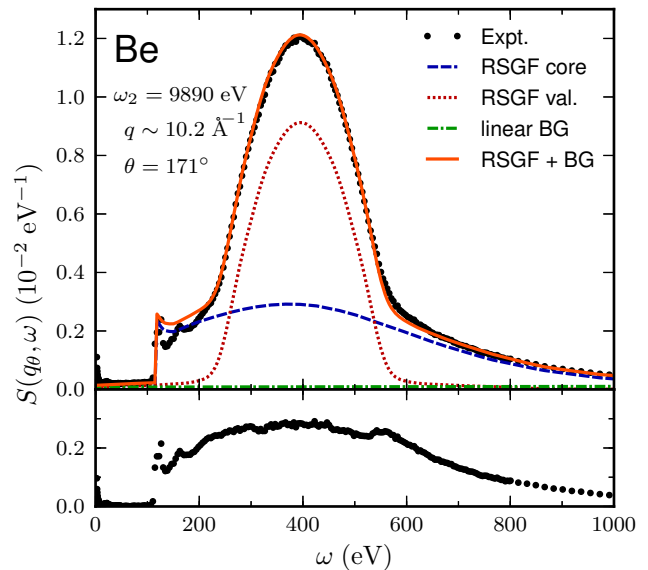


FIG. 1. (Color online.) XRTS from polycrystalline beryllium under ambient conditions at a fixed  $171^\circ$  scattering angle and 9890-eV scattered photon energy<sup>64</sup>. Here, the energy transfer  $\omega$  is the difference between the incident and scattered photon energies. In the upper panel, the data are shown along with a combined real-space Green's function (RSGF) valence and core calculation. The data have been scaled as described in the text. In the lower panel, the valence contribution and linear background have been subtracted to give the core contribution alone.

to first validate theoretical methodology against spectra taken under known thermodynamic conditions and at higher resolution than presently typical of WDM experiments. To this end, experimental XRTS data for polycrystalline Be at ambient temperature and pressure were collected using the lower energy resolution inelastic x-ray (LERIX) spectrometer at beamline 20-ID of the Advanced Photon Source.<sup>65</sup> Scattered photons with  $\omega_2 = (9891.7 \pm 0.2)$  eV were analyzed by a single spherically bent Si crystal located at a fixed  $171^\circ$  scattering angle while scanning the incident photon energy. From the elastic peak width the total instrumental resolution was determined to be 1.3 eV. The data, which have previously been reported<sup>64</sup>, are shown in Fig. 1. The graph is labelled  $S(q_0, \omega)$  to indicate that the data are collected at fixed scattering angle, and thus  $q$  is a weak function of  $\omega$ .

After normalizing to the incident flux, a small linear background and a single scale factor were fit in order to match the RSGF core calculation in the tail region ( $800 < \omega < 1500$  eV) and thus put the data into absolute units. The results of this fit have been used to scale the experimental data in Fig. 1. Additionally, theoretical core and valence calculations, the fit linear background, and the sum of these three are shown.



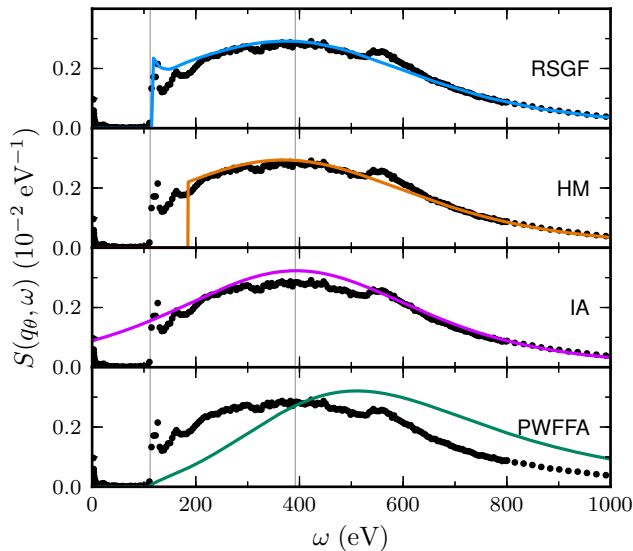


FIG. 2. (Color online.) Comparison of extracted core-shell XRTS with theoretical calculations using the RSGF, the hydrogenic model (HM), impulse approximation (IA), and plane-wave form-factor approximation (PWFFA). The energy transfer  $\omega$  is the difference between the incident and scattered photon energies. *All calculations are in absolute units.* Vertical guides are shown at the  $1s$  binding energy (112 eV) and the free-particle Compton shift (396 eV).

The experimental generalized oscillator strength  $\int (2/q^2)\omega S(q, \omega) d\omega$  matches that for the combined theoretical RSGF spectrum to within 1%. Since the measurement was performed at fixed scattering angle, this value is slightly larger than the Bethe  $f$ -sum rule<sup>18,66,67</sup> value of  $N=4$  (which only holds for experiments performed at fixed  $q$ ).

The theoretical valence profile, calculated from the RSGF,<sup>64</sup> was then subtracted to obtain the experimental core profile, shown in the lower panel of Fig. 1. The small peak visible for  $550 < \omega < 650$  eV is a result of the theoretical valence profile underestimating the actual contribution in this region, as was also seen in comparisons with higher momentum-transfer data (see Figs. 4 and 5 of Mattern, et al.<sup>64</sup>).

## IV. RESULTS AND DISCUSSION

### A. Comparison of Experiment and Theory

The extracted experimental core profile is compared in Fig. 2 to each of the four theoretical calculations discussed in Section II. All calculations are in absolute units and have taken the weak dependence of  $q$  on  $\omega$  into account. Vertical guides are included at the  $1s$  binding energy (112 eV) and the free-particle Compton shift (396 eV).

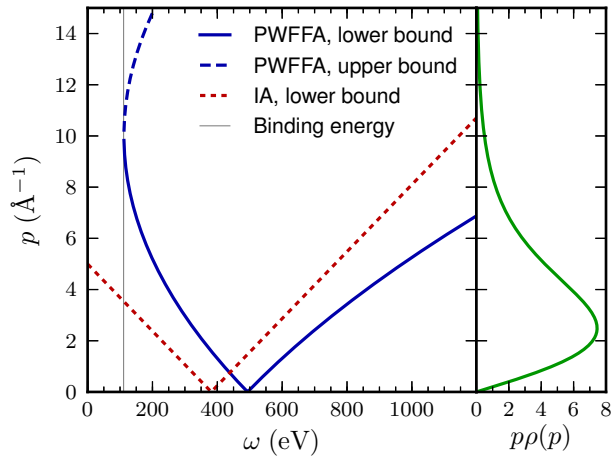


FIG. 3. (Color online.) On the left are shown the integration bounds for both the PWFFA (upper and lower bounds) and IA (lower only, upper bound is  $\infty$ ) calculations. On the right, plotted vertically, is the integrand  $p\rho(p)$ . Both the offset of the peak by the binding energy (112 eV) and the lack of convergence of the PWFFA to the IA at large  $\omega$  are apparent.

The IA and PWFFA calculations use the ground-state Dirac-Fock Be  $1s$  wavefunction calculated using FEFF's atomic solver as the initial state, and thus only differ in their treatment of the final states and energy conservation. For the RSGF calculation, the Dirac-Fock wavefunction is calculated in the presence of a  $1s$  core-hole. We have included only the atomic background contribution  $S_0(q, \omega)$ . The fine structure visible in the experimental data for  $\omega \lesssim 200$  eV is not included, although it has been treated elsewhere.<sup>58</sup> The HM calculation uses hydrogenic wavefunctions with an effective nuclear charge ( $Z=3.685$ )<sup>57</sup> for the initial and final states.

We focus on three regions for comparison: the vicinities of the  $K$ -edge binding energy ( $\omega \sim 112$  eV), the peak ( $\omega \sim 396$  eV), and the tail ( $\omega \gtrsim 600$  eV). The RSGF calculation matches the data reasonably well in all three regions (with the exception of immediately above the  $K$  edge, where interference effects have been omitted). The HM accurately describes the peak and tail regions, but shows a large deficit above the experimental binding energy due to the larger binding energy of the hydrogenic state. The IA, which ignores the binding energy, has an unphysical tail at low energy transfers. The peak region is reasonably well described by the IA, while the high- $\omega$  tail region is quite accurate. This is expected since the conditions of applicability of the IA are well satisfied for large energy transfer.

By contrast, although the PWFFA of Schumacher, et al.<sup>19</sup> vanishes below  $K$  edge, it exhibits only a gradual onset and further shows strong quantitative and qualitative disagreement with the experimental data everywhere else. Given its application in the interpretation of several XRTS experiments<sup>17,20-25</sup> on WDM, and its evident failure to describe high-resolution synchrotron measure-

ments, we now turn our focus to the PWFFA. We will first look in more detail at the source of the approximation's error, and then briefly discuss the possible implications for interpretation of experiment and future best practice.

### B. A closer look at the PWFFA

Although others have previously observed that the PWFFA gives results with unphysical features that are in disagreement with experimental data,<sup>68,69</sup> we are unaware of a discussion of the origin of the approximation's inconsistency. We now consider this point in detail.

An alternative route to obtain the PWFFA is to follow the IA derivation up to Eq. (5). At this point, if one makes the *ad hoc* approximation of replacing only the second  $H$  by  $H_0$ ,

$$S_i(\vec{q}, \omega) \approx \int \frac{dt}{2\pi} e^{i\omega t} \langle i | e^{iHt} e^{-i\vec{q}\cdot\vec{r}} e^{-iH_0 t} e^{i\vec{q}\cdot\vec{r}} | i \rangle. \quad (14)$$

then, instead, the PWFFA result (11) follows. Thus, the assumptions (9) correspond to making the uncontrolled approximation of evaluating the initial-state energy using  $H$  and the final-state energy using  $H_0$ . This effectively violates energy conservation, opening the possibility of unphysical results.

As we mentioned in Sect. IIC, the IA (6) and PWFFA (11) results differ only in the bounds of the integration over the momentum density. In left panel of Fig. 3, we show the integration bounds as a function of  $\omega$  for both theories. For the IA, there is no upper bound, and for the PWFFA the upper bound is only relevant for small  $\omega$ , beyond which it is well above the integrand's region of support. The right panel shows the integrand (rotated so that the abscissa runs vertically). The scattering spectra can be seen to peak when the lower integration bound vanishes. For the PWFFA, this is offset to higher energy transfer by the binding energy of the initial state. Furthermore, the failure of the PWFFA to reduce to the IA at large  $\omega$  can be clearly seen here. The offset of the PWFFA peak relative to the IA appears to be in conflict with the calculations presented in Fig. 3 of Riley, et al.<sup>20</sup>.

Given the much lower energy resolution typical of WDM experiments, it is natural to ask whether the discrepancies seen above are relevant in that context. In Fig. 4, we compare RSGF, IA and PWFFA calculations at the representative experimental conditions of Fortmann, et al.<sup>17</sup>. The IA calculation has been truncated at the empirical binding energy. In addition to the absolute-unit PWFFA calculation, we have included a curve scaled to match the  $f$ -sum of the other theoretical curves. The unbroadened calculations are shown in the upper panel. The curves in the middle panel are broadened by 115-eV (FWHM) to match the experimental resolution of Ref. 17. Finally, for illustrative purposes, the lower panel contains curves broadened by 500 eV. Even in the latter,

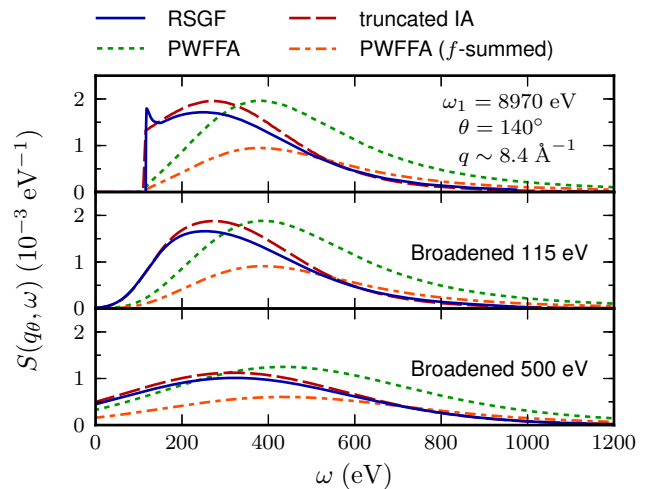


FIG. 4. (Color online.) Theoretical core profiles for the experimental conditions of Fortmann, et al.<sup>17</sup>. The inaccuracy of the PWFFA remains, even after substantial broadening.

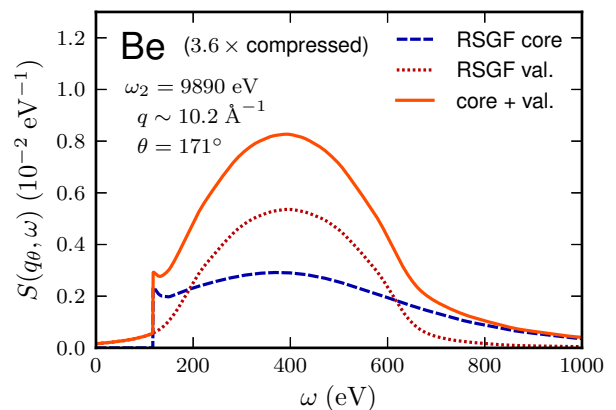


FIG. 5. (Color online.) Theoretical (RSGF) XRTS from polycrystalline Be compressed to  $3.6\times$  ambient density. The valence contribution is broader than under ambient conditions (*cf.* Fig. 1, top panel). Subsequently, the core contribution (assumed here to be independent of density) is relatively larger in the region of the peak.

admittedly extreme case, the PWFFA offset and subsequent overestimation of the high- $\omega$  tail is still quite prominent. The *ad hoc*  $f$ -sum scaling results in a tail that is only slightly overestimated, but at the cost of an extreme deficit beneath the peak.

At the higher densities typical of WDM, the core contribution becomes even more important. As the density is increased, the Fermi level increases relative to the bottom of the valence band resulting in a broader valence contribution. The core wavefunction, on the other hand, is only weakly dependent on density (at least for modest compression, where the cores from neighboring sites

have negligible overlap). Subsequently, as shown in Fig. 5 (*cf.* Fig. 1, top panel), the core contribution is relatively larger in the peak region, increasing the importance of a numerically accurate theoretical treatment.

### C. Implications

We now turn to implications of an incorrect core treatment on the interpretation of XRTS spectra from WDM. It is important to recognize the difficulty of these experiments and their analysis. The intrinsic width of back-lighter x-ray sources fundamentally limits the energy resolution obtainable in this measurement technique. The low flux and need for single-shot measurement requires the use of low-resolution spectrometers with limited spectral range further decreasing the resolution while also complicating background characterization. This uncertainty in the background subtraction makes  $f$ -sum normalization especially difficult, and thus the spectra often can not be reliably placed into absolute units. Furthermore, the highest likelihood background is necessarily dependent upon assumptions made about the core contribution to the spectrum.

The complicated interplay between the various degrees of freedom present in such fits makes it difficult to state the exact implications of using the PWFFA in the extraction of thermodynamic state variables in published work.<sup>17,20–25</sup> It is likely that, in order for a good fit in the high- $\omega$  tail to be obtained, the ionization state must be overestimated. This could explain the discrepancy noted by Fortmann, et al.,<sup>17</sup> between their best-fit ionization state found using the PWFFA and earlier work that appears to use the HM.<sup>70,71</sup> Beyond that, the net effect on extracted thermodynamic parameters is unclear. However, due to this previously undiagnosed systematic uncertainty, re-evaluation of existing experimental data<sup>17,20–25</sup> using a more appropriate core calculation and a maximum likelihood treatment of the background is necessary.

### D. Future Practice

The limitations of the PWFFA bring up the question of best future practice for fitting the core-shell XRTS from WDM. This will become particularly important when higher resolution WDM-XRTS experiments are performed at the Linac Coherent Light Source and the National Ignition Facility. If such experiments are to reach their full scientific potential, errors on the scale of those given by the PWFFA must be avoided. An ideal treatment would include self-consistent determination of occupied and unoccupied electronic states including condensed-phase effects. Also, the decrease of ionization potentials with increased density (*i.e.*, *continuum lowering*) should be either implicitly present in the calculation, or tunable using models from plasma physics.<sup>72–74</sup>

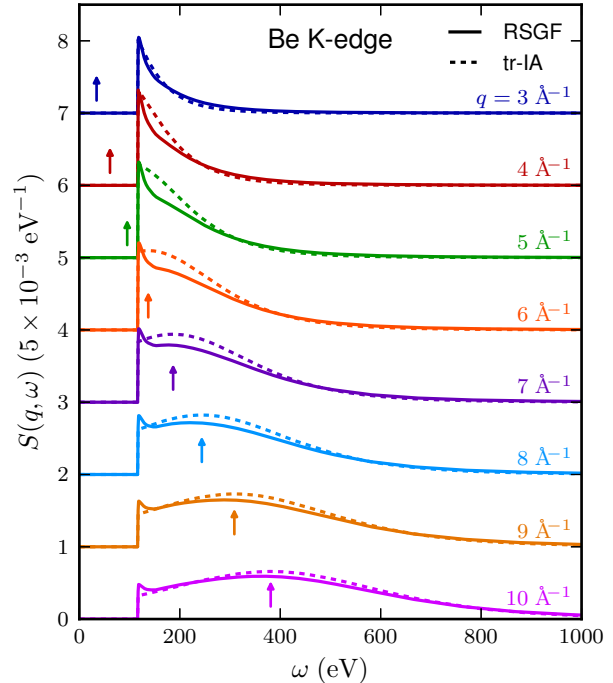


FIG. 6. (Color online.) Comparison of theoretical core contribution to Be  $K$ -edge XRTS calculated using RSGF and truncated IA methods as a function of momentum transfer. Vertical arrows are located at the free-particle Compton shifts.

Of the methods we have presented, the RSGF calculation most closely describes the ambient experimental data. Condensed-phase effects are included explicitly in final states. Although a frozen atomic core wavefunction is used, this is a common feature of all techniques under consideration, and should be sufficient at modest densities where core overlap is expected to be negligible. The primary limitation of the RSGF approach is that it is currently unclear how to incorporate continuum-lowering effects.

Alternatively, one can use an *ad hoc* modification of the low-energy-transfer tail of the IA

$$S_{\text{tr-IA}}(q, \omega) = S(q, \omega) \left( 1 - \frac{1}{e^{\beta(\omega - E_B)} + 1} \right). \quad (15)$$

We will refer to this approach, which for  $T = 0$  simply truncates the spectrum below binding energy, as the *truncated IA* (tr-IA). This allows straightforward application of continuum-lowering models to adjust the binding energy. A similar approach, using screened hydrogenic wavefunctions for the initial state instead of Dirac-Fock is discussed in Gregori, et al.<sup>75</sup>, but only in the context of smaller  $q$ , where the core contribution is relatively small. In Figs. 6, 7, and 8, we explore the accuracy and applicability of the tr-IA at  $T=0$  by comparing it with RSGF calculations for a range of momentum transfers for the  $K$

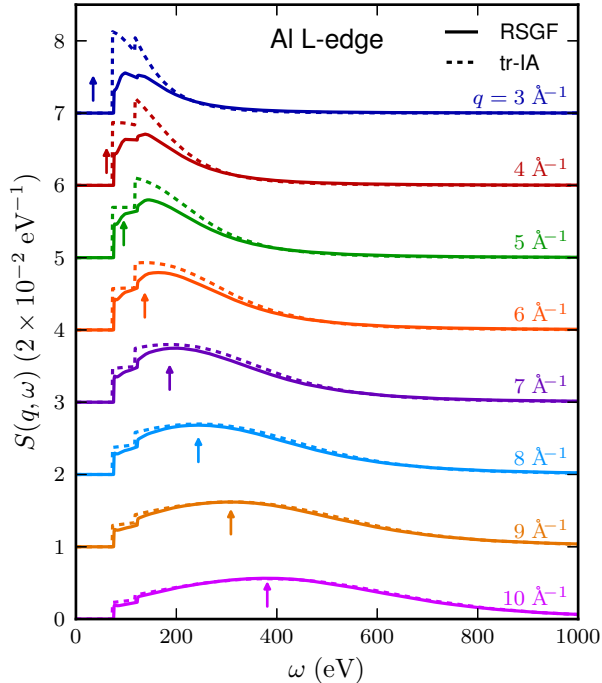


FIG. 7. (Color online.) Same as Fig. 6, except for Al  $L_{1-}$  and  $L_{2,3}$ -edge XRTS.

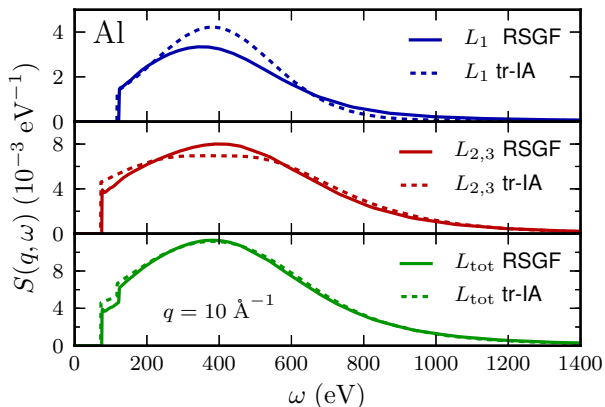


FIG. 8. (Color online.) Comparison of RSGF and IA calculations for  $L_1$  ( $2s$ ) and  $L_{2,3}$  ( $2p$ ) subshells, along with the combined spectra at high  $q$ . While the RSGF and IA differ for individual subshells, agreement is recovered for the combined spectra.

shell of Be and  $L$  shell of Al. Note that all calculations are in absolute units.

As long as the free-particle Compton shift (shown by vertical arrows) is a few times the edge energy, the tr-IA is in reasonable agreement with the RSGF calculation. Since the IA satisfies the  $f$ -sum rule by construction,

the truncation of the low  $\omega$  tail results in slight  $f$ -sum violations ( $\lesssim 5\%$  for Al,  $q \geq 6 \text{ \AA}^{-1}$ ). We also note that for the Al  $L$  shell, the tr-IA and RSGF calculations differ for the individual subshells (Fig. 8, upper two panels). However, agreement is recovered after combining to form the total  $L$ -shell contribution (Fig. 8 lower panel).

Recently, another approach to modeling XRTS from WDM has been discussed by Johnson, et al.<sup>76</sup> They use an *average-atom* model, which gives a significant improvement in the treatment of the free-electrons compared to a simple jellium model. Unfortunately, the average-atom binding energies disagree significantly with experiment, limiting the accuracy of the bound-free contribution to the XRTS spectrum. Johnson, et al.<sup>76</sup> also consider applying the PWFFA to the average-atom  $1s$  state for Be and find similar qualitative discrepancies as we have discussed here.

In summary, for XRTS experiments with modest energy resolution at high momentum transfer it should be sufficient to treat the bound-free contribution with a truncated IA, where the truncation energy is adjusted to include the effects of continuum lowering. However, the IA ceases to be accurate at lower momentum transfers. If continuum-lowering shifts and temperatures are negligible compared to the desired energy resolution, then the RSGF approach can be immediately applied at any momentum transfer. Further investigation is needed to determine if continuum lowering can be calculated or included empirically within the RSGF framework.

## V. CONCLUSION

We have discussed several techniques for calculating the core-shell contribution to XRTS and compared with experimental data collected from polycrystalline Be under ambient conditions. Of the techniques considered, the real-space Green's function method best describes the data. However, a simple *ad hoc* truncation of the impulse approximation is reasonably accurate at higher momentum transfers and allows more straightforward inclusion of continuum lower effects. The accuracy of this truncated IA as a function of  $q$  has been explored by comparing with RSGF calculations for both the Be  $K$ -shell and Al  $L$ -shell. On the other hand, the plane-wave form-factor approximation, which has been used in the interpretation of several WDM experiments<sup>17,20-25</sup> is quantitatively and qualitatively inaccurate due to an inconsistent treatment of the single-particle Hamiltonian. Re-evaluation of the experimental data using a more accurate core calculation and maximum likelihood background subtraction is recommended. More importantly, an accurate treatment of the bound-free XRTS from WDM will be necessary when higher resolution experiments are performed at the Linac Coherent Light Source and the National Ignition Facility. We believe we have also motivated the need for cross-method comparisons and the usefulness of exchange of both theoretical and



experimental techniques between the condensed-matter and dense-plasma communities.

## ACKNOWLEDGMENTS

This work was supported by the US Department of Energy, Office of Science, Fusion Energy Sciences and the National Nuclear Security Administration, through grant de-sc0008580. We thank C. Fortmann, S. Glenzer, G. Gregori, T. Döppner, J. Rehr, J. Kas, F. Vila and D. Riley for many enlightening discussions.

- <sup>1</sup>G. Gregori, S. H. Glenzer, W. Rozmus, R. W. Lee, and O. L. Landen, *Phys. Rev. E* **67**, 026412 (2003).
- <sup>2</sup>G. Gregori, S. H. Glenzer, and O. L. Landen, *Phys. Rev. E* **74**, 026402 (2006).
- <sup>3</sup>J. W. Dufty and S. B. Trickey, *Phys. Rev. B* **84**, 125118 (2011).
- <sup>4</sup>T. Sjostrom, F. E. Harris, and S. B. Trickey, *Phys. Rev. B* **85**, 045125 (2012).
- <sup>5</sup>K.-U. Plagemann, P. Sperling, R. Thiele, M. P. Desjarlais, C. Fortmann, T. Döppner, H. J. Lee, S. H. Glenzer, and R. Redmer, *New Journal of Physics* **14**, 055020 (2012).
- <sup>6</sup>G. Gregori, S. H. Glenzer, K. B. Fournier, K. M. Campbell, E. L. Dewald, O. S. Jones, J. H. Hammer, S. B. Hansen, R. J. Wallace, and O. L. Landen, *Phys. Rev. Lett.* **101**, 045003 (2008).
- <sup>7</sup>J. MacFarlane, I. Golovkin, and P. Woodruff, *Journal of Quantitative Spectroscopy and Radiative Transfer* **99**, 381 (2006).
- <sup>8</sup>J. D. Lindl, P. Amendt, R. L. Berger, S. G. Glendinning, S. H. Glenzer, S. W. Haan, R. L. Kauffman, O. L. Landen, and L. J. Suter, *Physics of Plasmas* **11**, 339 (2004).
- <sup>9</sup>B. A. Remington, R. P. Drake, and D. D. Ryutov, *Rev. Mod. Phys.* **78**, 755 (2006).
- <sup>10</sup>H. F. Wilson and B. Militzer, *Phys. Rev. Lett.* **108**, 111101 (2012).
- <sup>11</sup>E. I. Moses, R. N. Boyd, B. A. Remington, C. J. Keane, and R. Al-Ayat, *Physics of Plasmas* **16**, 041006 (2009).
- <sup>12</sup>T. Döppner, O. Landen, H. Lee, P. Neumayer, S. Regan, and S. H. Glenzer, *High Energy Density Physics* **5**, 182 (2009).
- <sup>13</sup>R. A. Forman, G. J. Piermarini, J. D. Barnett, and S. Block, *Science* **176**, 284 (1972).
- <sup>14</sup>G. J. Piermarini, S. Block, J. D. Barnett, and R. A. Forman, *Journal of Applied Physics* **46**, 2774 (1975).
- <sup>15</sup>Y. M. Gupta and X. A. Shen, *Applied Physics Letters* **58**, 583 (1991).
- <sup>16</sup>D. D. Ragan, R. Gustavsen, and D. Schiferl, *Journal of Applied Physics* **72**, 5539 (1992).
- <sup>17</sup>C. Fortmann, H. J. Lee, T. Döppner, R. W. Falcone, A. L. Kritcher, O. L. Landen, and S. H. Glenzer, *Phys. Rev. Lett.* **108**, 175006 (2012).
- <sup>18</sup>W. Schülke, *Electron Dynamics by Inelastic X-Ray Scattering*, Oxford Series on Synchrotron Radiation (Oxford University Press, New York, 2007).
- <sup>19</sup>M. Schumacher, F. Smend, and I. Borchert, *Journal of Physics B: Atomic and Molecular Physics* **8**, 1428 (1975).
- <sup>20</sup>D. Riley, F. Khattak, E. Garcia Saiz, G. Gregori, S. Bandyopadhyay, M. Notley, D. Neely, D. Chambers, A. Moore, and A. Comley, *Laser and Particle Beams* **25**, 465 (2007).
- <sup>21</sup>H. Sawada, S. P. Regan, D. D. Meyerhofer, I. V. Igumenshchev, V. N. Goncharov, T. R. Boehly, R. Epstein, T. C. Sangster, V. A. Smalyuk, B. Yaakobi, G. Gregori, S. H. Glenzer, and O. L. Landen, *Physics of Plasmas* **14**, 122703 (2007).
- <sup>22</sup>S. Sahoo, G. F. Gribakin, G. Shabbir Naz, J. Kohanoff, and D. Riley, *Phys. Rev. E* **77**, 046402 (2008).
- <sup>23</sup>S. H. Glenzer and R. Redmer, *Reviews of Modern Physics* **81**, 1625 (2009).
- <sup>24</sup>A. L. Kritcher, P. Neumayer, C. R. D. Brown, P. Davis, T. Döppner, R. W. Falcone, D. O. Gericke, G. Gregori, B. Holst, O. L. Landen, H. J. Lee, E. C. Morse, A. Pelka, R. Redmer, M. Roth, J. Vorberger, K. Wünsch, and S. H. Glenzer, *Phys. Rev. Lett.* **103**, 245004 (2009).
- <sup>25</sup>A. L. Kritcher, T. Döppner, C. Fortmann, T. Ma, O. L. Landen, R. Wallace, and S. H. Glenzer, *Phys. Rev. Lett.* **107**, 015002 (2011).
- <sup>26</sup>S. P. Hau-Riege, A. Graf, T. Döppner, R. A. London, J. Krzywinski, C. Fortmann, S. H. Glenzer, M. Frank, K. Sokolowski-Tinten, M. Messerschmidt, C. Bostedt, S. Schorb, J. A. Bradley, A. Lutman, D. Rolles, A. Rudenko, and B. Rudek, *Phys. Rev. Lett.* **108**, 217402 (2012).
- <sup>27</sup>U. Zastra, P. Audebert, V. Bernshtam, E. Brambrink, T. Kämpfer, E. Kroupp, R. Loetzsch, Y. Maron, Y. Ralchenko, H. Reinholz, G. Röpke, A. Sengebusch, E. Stambulchik, I. Uschmann, L. Weingarten, and E. Förster, *Phys. Rev. E* **81**, 026406 (2010).
- <sup>28</sup>A. Sengebusch, H. Reinholz, G. Röpke, U. Zastra, T. Kämpfer, I. Uschmann, E. Förster, E. Stambulchik, E. Kroupp, and Y. Maron, *Journal of Physics A: Mathematical and Theoretical* **42**, 214061 (2009).
- <sup>29</sup>E. Stambulchik, V. Bernshtam, L. Weingarten, E. Kroupp, D. Fisher, Y. Maron, U. Zastra, I. Uschmann, F. Zamponi, E. Förster, A. Sengebusch, H. Reinholz, G. Röpke, and Y. Ralchenko, *Journal of Physics A: Mathematical and Theoretical* **42**, 214056 (2009).
- <sup>30</sup>P. M. Nilson, A. A. Solodov, J. F. Myatt, W. Theobald, P. A. Jaanimagi, L. Gao, C. Stoeckl, R. S. Craxton, J. A. Delettrez, B. Yaakobi, J. D. Zuegel, B. E. Kruschwitz, C. Dorrer, J. H. Kelly, K. U. Akli, P. K. Patel, A. J. Mackinnon, R. Betti, T. C. Sangster, and D. D. Meyerhofer, *Phys. Rev. Lett.* **105**, 235001 (2010).
- <sup>31</sup>A. Lévy, F. Dorchies, A. Benuzzi-Mounaix, A. Ravasio, F. Festa, V. Recoules, O. Peyrusse, N. Amadou, E. Brambrink, T. Hall, M. Koenig, and S. Mazevet, *Phys. Rev. Lett.* **108**, 055002 (2012).
- <sup>32</sup>S. M. Vinko, O. Ciricosta, B. I. Cho, K. Engelhorn, H.-K. Chung, C. R. D. Brown, T. Burian, J. Chalupsky, R. W. Falcone, C. Graves, V. Hajkova, A. Higginbotham, L. Juha, J. Krzywinski, H. J. Lee, M. Messerschmidt, C. D. Murphy, Y. Ping, A. Scherz, W. Schlotter, S. Toleikis, J. J. Turner, L. Vysin, T. Wang, B. Wu, U. Zastra, D. Zhu, R. W. Lee, P. A. Heimann, B. Nagler, and J. S. Wark, *Nature* **482**, 59 (2012).
- <sup>33</sup>M. J. Cooper, P. E. Mijnders, N. Shiotani, N. Sakai, and A. Bansil, *X-Ray Compton Scattering*, Oxford Series on Synchrotron Radiation (Oxford University Press, 2004).
- <sup>34</sup>S. Huotari, C. Sternemann, M. Volmer, J. A. Soininen, G. Monaco, and W. Schülke, *Phys. Rev. B* **76**, 235106 (2007).
- <sup>35</sup>M. Volmer, C. Sternemann, J. S. Tse, T. Buslaps, N. Hiraoka, C. L. Bull, J. Gryko, P. F. McMillan, M. Paulus, and M. Tolan, *Phys. Rev. B* **76**, 233104 (2007).
- <sup>36</sup>S. Huotari, J. A. Soininen, T. Pyllkänen, K. Hämäläinen, A. Issolah, A. Titov, J. McMinis, J. Kim, K. Esler, D. M. Ceperley, M. Holzmann, and V. Olevano, *Physical Review Letters* **105**, 086403 (2010).
- <sup>37</sup>S. Huotari, B. Boldrini, V. Honkimäki, P. Suortti, and W. Weyrich, *Journal of Synchrotron Radiation* **16**, 672 (2009).
- <sup>38</sup>M. Hakala, S. Huotari, K. Hämäläinen, S. Manninen, P. Wernet, A. Nilsson, and L. G. M. Pettersson, *Phys. Rev. B* **70**, 125413 (2004).
- <sup>39</sup>J. T. Okada, P. H.-L. Sit, Y. Watanabe, Y. J. Wang, B. Barbiellini, T. Ishikawa, M. Itou, Y. Sakurai, A. Bansil, R. Ishikawa, M. Hamaishi, T. Masaki, P.-F. Paradis, K. Kimura, T. Ishikawa, and S. Nanao, *Physical Review Letters* **108**, 067402 (2012).
- <sup>40</sup>Y. Sakurai, M. Itou, B. Barbiellini, P. E. Mijnders, R. S. Markiewicz, S. Kaprzyk, J.-M. Gillet, S. Wakimoto, M. Fujita, S. Basak, Y. J. Wang, W. Al-Sawai, H. Lin, A. Bansil, and K. Yamada, *Science* **332**, 698 (2011).
- <sup>41</sup>J. A. Bradley, A. Sakko, G. T. Seidler, A. Rubio, M. Hakala, K. Hämäläinen, G. Cooper, A. P. Hitchcock, K. Schlimmer, and K. P. Nagle, *Phys. Rev. A* **84**, 022510 (2011).

- <sup>42</sup>J. A. Bradley, P. Yang, E. R. Batista, K. S. Boland, C. J. Burns, D. L. Clark, S. D. Conradson, S. A. Kozimor, R. L. Martin, G. T. Seidler, B. L. Scott, D. K. Shuh, T. Tylliszczak, M. P. Wilkerson, and L. E. Wolfsberg, *Journal of the American Chemical Society* **132**, 13914 (2010).
- <sup>43</sup>J. A. Bradley, G. T. Seidler, G. Cooper, M. Vos, A. P. Hitchcock, A. P. Sorini, C. Schlimmer, and K. P. Nagle, *Phys. Rev. Lett.* **105**, 053202 (2010).
- <sup>44</sup>A. Sakko, C. Sternemann, C. J. Sahle, H. Sternemann, O. M. Feroughi, H. Conrad, F. Djurabekova, A. Hohl, G. T. Seidler, M. Tolan, and K. Hämäläinen, *Physical Review B* **81**, 205317 (2010).
- <sup>45</sup>O. M. Feroughi, C. Sternemann, C. J. Sahle, M. A. Schroer, H. Sternemann, H. Conrad, A. Hohl, G. T. Seidler, J. Bradley, T. T. Fister, M. Balasubramanian, A. Sakko, K. Pirkkalainen, K. Hämäläinen, and M. Tolan, *Applied Physics Letters* **96**, 081912 (2010).
- <sup>46</sup>H. Sternemann, C. Sternemann, G. T. Seidler, T. T. Fister, A. Sakko, and M. Tolan, *Journal of Synchrotron Radiation* **15**, 162 (2008).
- <sup>47</sup>T. T. Fister, F. D. Vila, G. T. Seidler, L. Svec, J. C. Linehan, and J. O. Cross, *Journal of the American Chemical Society* **130**, 925 (2008).
- <sup>48</sup>R. A. Gordon, G. T. Seidler, T. T. Fister, M. W. Haverkort, G. A. Sawatzky, A. Tanaka, and T. K. Sham, *EPL (Europhysics Letters)* **81**, 26004 (2008).
- <sup>49</sup>M. Balasubramanian, C. S. Johnson, J. O. Cross, G. T. Seidler, T. T. Fister, E. A. Stern, C. Hamner, and S. O. Mariager, *Applied Physics Letters* **91**, 031904 (2007).
- <sup>50</sup>T. T. Fister, G. T. Seidler, C. Hamner, J. O. Cross, J. A. Soininen, and J. J. Rehr, *Phys. Rev. B* **74**, 214117 (2006).
- <sup>51</sup>Y. Feng, G. T. Seidler, J. O. Cross, A. T. Macrander, and J. J. Rehr, *Phys. Rev. B* **69**, 125402 (2004).
- <sup>52</sup>S. K. Lee, J.-F. Lin, Y. Q. Cai, N. Hiraoka, P. J. Eng, T. Okuchi, H.-k. Mao, Y. Meng, M. Y. Hu, P. Chow, J. Shu, B. Li, H. Fukui, B. H. Lee, H. N. Kim, and C.-S. Yoo, *Proceedings of the National Academy of Sciences* **105**, 7925 (2008).
- <sup>53</sup>P. Wernet, D. Nordlund, U. Bergmann, M. Cavalleri, M. Odelius, H. Ogasawara, L. Naslund, T. Hirsch, L. Ojamae, P. Glatzel, L. Pettersson, and A. Nilsson, *Science* **304**, 995 (2004).
- <sup>54</sup>J. J. Rehr and R. C. Albers, *Reviews of Modern Physics* **72**, 621 (2000).
- <sup>55</sup>J. J. Rehr, J. J. Kas, M. P. Prange, A. P. Sorini, Y. Takimoto, and F. Vila, *Comptes Rendus Physique* **10**, 548 (2009).
- <sup>56</sup>P. Eisenberger and P. M. Platzman, *Physical Review A* **2**, 415 (1970).
- <sup>57</sup>E. Clementi and D. L. Raimondi, *The Journal of Chemical Physics* **38**, 2686 (1963).
- <sup>58</sup>J. A. Soininen, A. L. Ankudinov, and J. J. Rehr, *Physical Review B* **72**, 045136 (2005).
- <sup>59</sup>H. Sternemann, C. Sternemann, J. S. Tse, S. Desgreniers, Y. Q. Cai, G. Vankó, N. Hiraoka, A. Schacht, J. A. Soininen, and M. Tolan, *Phys. Rev. B* **75**, 245102 (2007).
- <sup>60</sup>H. Sternemann, J. A. Soininen, C. Sternemann, K. Hämäläinen, and M. Tolan, *Phys. Rev. B* **75**, 075118 (2007).
- <sup>61</sup>Y. Feng, J. A. Soininen, A. L. Ankudinov, J. O. Cross, G. T. Seidler, A. T. Macrander, J. J. Rehr, and E. L. Shirley, *Phys. Rev. B* **77**, 165202 (2008).
- <sup>62</sup>T. T. Fister, K. P. Nagle, F. D. Vila, G. T. Seidler, C. Hamner, J. O. Cross, and J. J. Rehr, *Phys. Rev. B* **79**, 174117 (2009).
- <sup>63</sup>T. Pylkkanen, V. M. Giordano, J.-C. Chervin, A. Sakko, M. Hakala, J. A. Soininen, K. Hamalainen, G. Monaco, and S. Huotari, *The Journal of Physical Chemistry B* **114**, 3804 (2010).
- <sup>64</sup>B. A. Mattern, G. T. Seidler, J. J. Kas, J. I. Pacold, and J. J. Rehr, *Physical Review B* **85**, 115135 (2012).
- <sup>65</sup>T. T. Fister, G. T. Seidler, L. Wharton, A. R. Battle, T. B. Ellis, J. O. Cross, A. T. Macrander, W. T. Elam, T. A. Tyson, and Q. Qian, *Review of Scientific Instruments* **77**, 063901 (2006).
- <sup>66</sup>M. Inokuti, Y. Itikawa, and J. E. Turner, *Rev. Mod. Phys.* **50**, 23 (1978).
- <sup>67</sup>S. Wang, *Phys. Rev. A* **60**, 262 (1999).
- <sup>68</sup>R. Currat, P. D. DeCicco, and R. Kaplow, *Phys. Rev. B* **3**, 243 (1971).
- <sup>69</sup>F. Bell, *Zeitschrift für Physik D* **3**, 97 (1986).
- <sup>70</sup>H. J. Lee, P. Neumayer, J. Castor, T. Döppner, R. W. Falcone, C. Fortmann, B. A. Hammel, A. L. Kritcher, O. L. Landen, R. W. Lee, D. D. Meyerhofer, D. H. Munro, R. Redmer, S. P. Regan, S. Weber, and S. H. Glenzer, *Phys. Rev. Lett.* **102**, 115001 (2009).
- <sup>71</sup>S. Glenzer, H. Lee, P. Davis, T. Döppner, R. Falcone, C. Fortmann, B. Hammel, A. Kritcher, O. Landen, R. Lee, D. Munro, R. Redmer, and S. Weber, *High Energy Density Physics* **6**, 1 (2010).
- <sup>72</sup>G. Ecker and W. Kroll, *Physics of Fluids* **6**, 62 (1963).
- <sup>73</sup>J. C. Stewart and K. D. Pyatt, Jr., *Astrophys. J.* **144**, 1203 (1966).
- <sup>74</sup>G. Zimmerman and R. More, *Journal of Quantitative Spectroscopy and Radiative Transfer* **23**, 517 (1980).
- <sup>75</sup>G. Gregori, S. H. Glenzer, F. J. Rogers, S. M. Pollaine, O. L. Landen, C. Blancard, G. Faussurier, P. Renaudin, S. Kuhlbrodt, and R. Redmer, *Physics of Plasmas* **11**, 2754 (2004).
- <sup>76</sup>W. R. Johnson, J. Nilsen, and K. T. Cheng, *Phys. Rev. E* **86**, 036410 (2012).